Quantum Inception Score

Akira Sone,[1,*] Akira Tanji,[2] and Naoki Yamamoto[2,3,†]

[1]*Department of Physics, University of Massachusetts, Boston, Massachusetts 02125, USA*
[2]*Department of Applied Physics and Physico-Informatics, Keio University, Hiyoshi 3-14-1, Kohoku, Yokohama 223-8522, Japan*
[3]*Keio Quantum Computing Center, Keio University, Hiyoshi 3-14-1, Kohoku, Yokohama 223-8522, Japan*

Motivated by the great success of classical generative models in machine learning, enthusiastic exploration of their quantum version has recently started. To depart on this journey, it is important to develop a relevant metric to evaluate the quality of quantum generative models; in the classical case, one such example is the inception score. In this paper, we propose the quantum inception score, which relates the quality to the Holevo information of the quantum channel that classifies a given dataset. We prove that, under this proposed measure, the quantum generative models provide better quality than their classical counterparts because of the presence of quantum coherence, characterized by the resource theory of asymmetry, and entanglement. Furthermore, we harness the quantum fluctuation theorem to characterize the physical limitation of the quality of quantum generative models. Finally, we apply the quantum inception score to assess the quality of the one-dimensional spin chain model as a quantum generative model, with the quantum convolutional neural network as a quantum classifier, for the phase classification problem in the quantum many-body physics.

arXiv:2311.12163v2 [quant-ph] 11 Mar 2024

I. Introduction

A burgeoning advancement of the artificial intelligence (AI) is a hallmark of the contemporary Information Age. The principal objective of AI research is the creation of machines which exhibit human-like capabilities of performing complicated tasks including learning, analyzing and reasoning. Presently, the prevailing landscape of AI technologies is predominantly underpinned by the machine learning algorithms, such as convolutional neural network and support vector machine, which have been embracing various applications [1–5]. However, recently, the machine learning has been warned to adhere to a Moore's law-like trend concerning the size of datasets [6], namely the curse of the dimensionality. Considering that people seek to encode data into larger feature spaces to facilitate pattern discovery, there is a pressing need for an alternative approach to reduce complexity in the context of big data analysis.

Quantum computers hold significant potential to attack such challenge, owing to their intrinsic greater information storage and information processing capacities compared to the classical devices [7]. Actually, we find enthusiastic exploration for the quantum-enhanced machine learning [8–12]. Especially our primary focus is on unsupervised learning [13, 14], which is a field dedicated to uncovering hidden patterns within unlabeled datasets and further classifying them. One of the most successful framework in classical unsupervised learning is the generative models [15, 16], where the generator and classifier are trained to produce data, such as images, with substantial diversity and high accuracy, respectively, from a vast amount of unlabeled data. The quality of the generative models is defined by the balance between the accuracy and diversity. Note that, in practice, the classifier is designed depending on the generator. Therefore, the primary objective of the generative models is to train the generator to achieve the well balanced accuracy and diversity, i.e., high quality. Prominent examples of the generative models include variational autoencoders (VAEs) [17] and generative adversarial networks (GANs) [18]. It is then important to have a relevant metric to evaluate the quality of the generative models, and the so-called *inception score (IS)* [19, 20] is an example of such metric. In practice, achieving a higher IS equates to better quality of the generative models that enjoys better balanced accuracy and diversity. Quantum generative models [21–23] serve as the quantum counterparts to classical generative models. Various quantum generative models have been proposed, which include variational quantum autoencoders (VQAEs) [24–27], the quantum generative adversarial networks (qGANs) [28–30] and quantum Boltzmann machines [31–33]. Furthermore, quantum generative models have recently found applications in various domains, such as quantum many-body physics [34–36].

To assess the quality of quantum generative models and highlight the factors that distinguish their performance compared to classical models, we need a meaningful and physically attainable metric. In this paper, we propose the *quantum inception score (qIS)*, which can be defined through the use of Holevo information [37, 38]. This allows us to connect the physical interpretation of the quality of generative models with the classical capacity of the quantum channel playing a role as a classifier. The proposed metric leads us to demonstrate that the quantum advantage in this metric is attributed to the presence of quantum coherence preserved by the quantum classifier, and further that the entanglement of the gen-

* akira.sone@umb.edu
† yamamoto@appi.keio.ac.jp

erator's output and the joint measurement on the classifier play a significant role in asymptotically achieving the best qIS. Our results not only serve as another illustrative example highlighting the advantage of quantum generative models arising from entanglement and coherence, but also support the claim by Gao *et al.* [22], demonstrating the enhancement of expressivity of the quantum generative models due to the Greenberger–Horne–Zeilinger (GHZ) state and cluster state, from a different perspective. Moreover, our results support the claim by Huang *et al.* [39], demonstrating the quantum advantage in learning achieved by the joint measurement. Moreover, leveraging the qIS, we employ the information-theoretic fluctuation theorem [40–42] to characterize the physical limitation of the quality of quantum generative models based on the concept of quantum efficacy [42–44]. Figure 1 presents four main results summarized in Def. 1 and Thms. 1, 2 and 3. Finally, we provide an example of applying the qIS to assess the power of the one-dimensional (1D) spin chain model combined with the quantum convolutional neural network (QCNN) [45, 46], for the phase classification problem. These results corroborate the significance of exploring the quantum foundation and communication approach to study the quantum machine learning protocols.

This paper is organized as follows. In Sec. II, we briefly review the concept of IS in the classical generative models and introduce the qIS in Sec. III. Then, we compare the qIS and cIS in Sec. IV, and further discuss the role of quantum coherence in Sec. V. Furthermore, we utilize the quantum fluctuation theorem to characterize the degradation of the quality in Sec. VI. Finally, we show the examples of using the qIS to assess the quantum generative models for the phase classification of the 1D spin-1/2 chain in Sec. VII, followed by the conclusion in Sec. VIII.

II. Inception score

Let us first review the concept of IS based on Refs. [19, 20]. Let $\mathcal{X} \equiv \{x_0, x_1, x_2 \cdots, x_{r-1}\}$ be a dataset produced from an unknown probability distribution. The aim of generative modeling is to construct a model $p(x)$ that approximates the unknown probability distribution producing $\mathcal{X}$. Here, let us consider the case that we want to evaluate the quality of a trained generative model which encodes a distribution $p(x)$ over the dataset $\mathcal{X}$. Given a data x_i, we also aim to construct a classifier that produces a relevant label $y_j \in \mathcal{Y} \equiv \{y_0, y_1, y_2, \cdots, y_{\ell-1}\}$, where ℓ denotes the number of the labels; we model the classifier via the conditional probability $p(y|x)$, which is usually constructed via a neural network. Note here that, in the generative models, we always have $\ell \leqslant r$. This is because we usually assume that the number of labels characterizing the patterns of the encoded dataset is smaller than that of the number of the input data. The marginal probability for the label data, $p(y_j)$, is given by $p(y_j) = \sum_{i=0}^{r-1} p(y_j|x_i)p(x_i)$. Therefore, the *input* and *output* of the network are $p(x_i)$ and $p(y_j)$, respectively. Then, the IS of $p(x)$ relative to $p(y|x)$ is defined by

$$\xi \equiv \exp\left(\sum_{i=0}^{r-1} p(x_i) D(p(y|x_i) \,\|\, p(y))\right), \tag{1}$$

where

$$D(p(y|x_i) \,\|\, p(y)) \equiv \sum_{j=0}^{\ell-1} p(y_j|x_i) \ln \frac{p(y_j|x_i)}{p(y_j)} \tag{2}$$

is the Kullback–Leibler (KL) divergence of the conditional label probability $p(y_j|x_i)$ with respect to $p(y_j)$. Note that $\ln \xi$ can be expressed as $\ln \xi = \sum_i p(x_i) \sum_j p(y_j|x_i) \ln p(y_j|x_i) - \sum_j p(y_j) \ln p(y_j)$, that is, the sum of the expected negative Shannon entropy of $p(y|x)$ and the entropy of $p(y)$. The former quantifies the accuracy of the label assigned to the data and the latter does the diversity of the data, implying that a generative model with bigger IS may cast as a high-quality data generator. Therefore, in this scenario, the primary objective is to construct generative models, with the help of relevant design of the classifier, that achieves the higher IS; for this reason, IS has been often used for GAN.

III. Quantum inception score

We consider a general setup of quantum generative model with a system described by d-dimensional Hilbert space $\mathcal{H}_S$. Let $\mathcal{B}(\mathcal{H}_S)$ denotes the set of density operators acting on $\mathcal{H}_S$. Suppose that the generator encodes a classical data $x_i \in \mathcal{X}$ to an input state $\rho_{\rm in}(x_i) \in \mathcal{B}(\mathcal{H}_S)$, for $i = 0, 1, 2, \cdots, (r-1)$. As in the usual machine learning scenario that tries to solve problems by encoding data into a larger dimensional space, we assume $d \geqslant r$. The encoded quantum states are then processed by a completely positive and trace-preserving (CPTP) map $\Phi : \mathcal{B}(\mathcal{H}_S) \to \mathcal{B}(\mathcal{H}'_S)$, where $\mathcal{H}'_S$ denotes the d'-dimensional Hilbert space of the output system. Thus the output state $\rho_{\rm out} \in \mathcal{B}(\mathcal{H}'_S)$ is related to the input as $\rho_{\rm out} = \Phi(\rho_{\rm in})$.

Now, let us write the input state $\rho_{\rm in}$ as an ensemble of $\rho_{\rm in}(x_i) \in \mathcal{B}(\mathcal{H}_S)$ encoding the classical input data $x_i \in \mathcal{X}$ sampled from a probability distribution $p(x_i)$, i.e.,

$$\rho_{\rm in} = \sum_{i=0}^{r-1} p(x_i) \rho_{\rm in}(x_i). \tag{3}$$

Note that in general $\rho_{\rm in}(x_i)$ does not necessarily commute with $\rho_{\rm in}(x_{i'})$ when $i \neq i'$. Then, the output state becomes

$$\rho_{\rm out} = \sum_{i=0}^{r-1} p(x_i) \rho_{\rm out}^{(i)}, \tag{4}$$

where

$$\rho_{\rm out}^{(i)} \equiv \Phi(\rho_{\rm in}(x_i)). \tag{5}$$

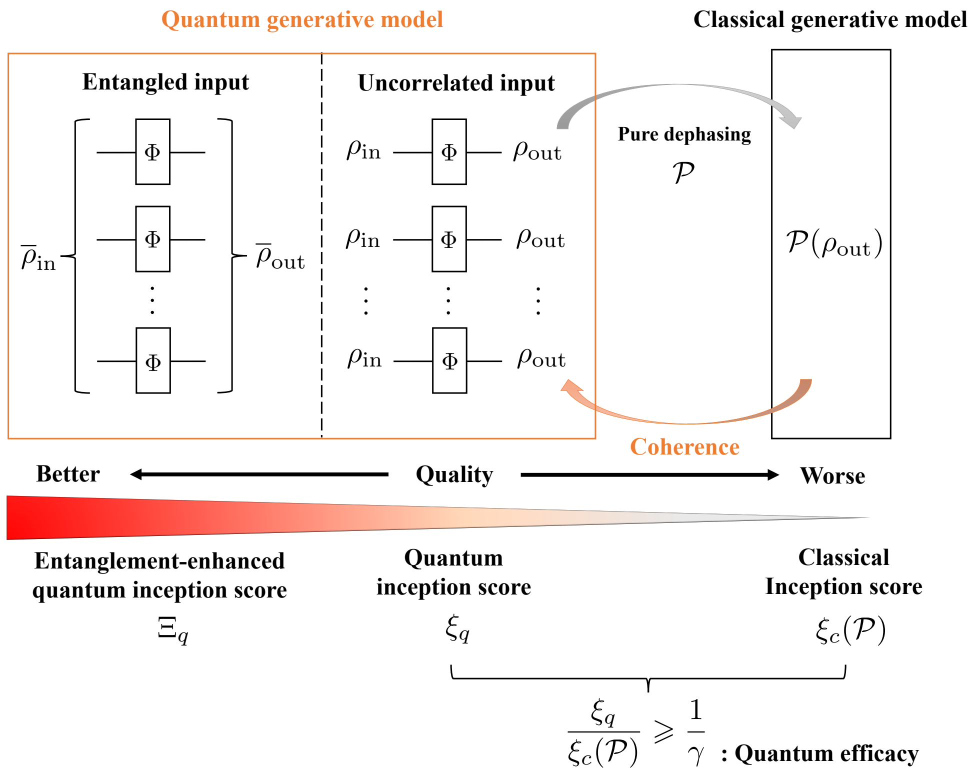

FIG. 1. Summary of the main results. We propose a definition of the quantum IS (Def. 1). Consequently, we demonstrate that the quality of the quantum generative model surpasses that of its classical counterpart (Thm. 1) due to the presence of quantum coherence (Thm. 2) preserved during the classification process. Additionally, we show that the quantum IS can be enhanced through entanglement of the generator's output and joint measurement on the classifier (Def. 2). Furthermore, by employing the quantum fluctuation theorem approach, we illustrate that the quality degrades due to pure dephasing in the quantum classifier, which can be characterized by the quantum efficacy (Thm. 3).

Let us write the ensemble of the output state as

$$\mathcal{E} \equiv \left\{ p(x_i), \rho_{\text{out}}^{(i)} \right\}_{i=0}^{r-1} . \tag{6}$$

Because the supports of $\rho_{\text{out}}^{(i)}$ and ρ_{out} satisfy $\text{supp}(\rho_{\text{out}}^{(i)}) \subseteq \text{supp}(\rho_{\text{out}})$, the quantum relative entropy $S(\rho_{\text{out}}^{(i)} \,\|\, \rho_{\text{out}}) \equiv \text{Tr}[\rho_{\text{out}}^{(i)} \ln \rho_{\text{out}}^{(i)}] - \text{Tr}[\rho_{\text{out}}^{(i)} \ln \rho_{\text{out}}]$ takes a finite value. Then the Holevo information $\chi(\mathcal{E}; \rho_{\text{out}})$ of the output ensemble is defined as [37, 38]

$$\chi(\mathcal{E}; \rho_{\text{out}}) \equiv \sum_{i=0}^{r-1} p(x_i) S(\rho_{\text{out}}^{(i)} \,\|\, \rho_{\text{out}}) . \tag{7}$$

The Holevo-Schumacher-Westmoreland (HSW) capacity (or Holevo capacity) [47–53] is defined as the maximization of the Holevo information over all the possible $p(x_i)$ and $\rho_{\text{in}}(x_i)$:

$$\chi_{\max}(\Phi) \equiv \max_{\{p(x_i), \rho_{\text{in}}(x_i)\}} \chi(\mathcal{E}; \rho_{\text{out}}) . \tag{8}$$

In the most generic scenario, the maximal transmittable amount of classical information through the quantum channel Φ is measured by the regularized classical capacity $C(\Phi)$ [51–55]

$$C(\Phi) \equiv \lim_{n \to \infty} \frac{1}{n} \chi_{\max}(\Phi^{\otimes n}) , \tag{9}$$

which is asymptotically achievable with infinite number of Φ, and we always have [52–55]

$$C(\Phi) \geqslant \chi_{\max}(\Phi) . \tag{10}$$

From these facts, as our *first main result*, we define the qIS as follows.

Definition 1 (Quantum Inception Score)**.** *The quantum inception score (qIS) is defined as*

$$\xi_q \equiv \exp\left(\chi(\mathcal{E}; \rho_{\text{out}}) \right) . \tag{11}$$

Suppose now that the task of quantum generator is to generate the optimal set of $\{p(x_i), \rho_{\text{in}}(x_i)\}$ to maximize ξ_q. Then, because the asymptotically achievable maximal qIS is given by $\exp(C(\Phi))$, from Eqs. (9) and (10), $\exp(C(\Phi))$ is regarded as an indicator of the best achievable quality by the quantum generator. Adopting an example of the image recognition, these results are consistent to the intuition that having a greater volume of information enables the generator to achieve better balanced accuracy and diversity.

Particularly, in the asymptotic setup, when the joint measurement on $\overline{\rho}_{\rm out} \equiv \Phi^{\otimes n}(\overline{\rho}_{\rm in})$ with entanglement input $\overline{\rho}_{\rm in} \in \mathcal{B}(\mathcal{H}_S^{\otimes n})$ is allowed, we always have $C(\Phi) > \chi_{\max}(\Phi)$ [54, 55]. With this special case, we define the maximally achievable qIS as follows.

Definition 2. *With the joint measurement and entanglement input, the maximally achievable qIS is given by*

$$\Xi_q \equiv \exp\left(C(\Phi)\right) , \tag{12}$$

which we call the entanglement-enhanced qIS.

Note that Eq. (9) still holds; therefore, the best quality is still asymptotically achievable. This result implies that the entanglement of the generator's output and joint measurement on the classifier play a significant role in achieving the best quality of the quantum generative models. This result can be regarded as an example supporting both the claim by Gao *et al.* [22], which demonstrated the quantum advantage of the quantum generative models thanks to the entanglement, and the claim by Huang *et al.* [39], which demonstrated the quantum advantage in learning achieved by the joint measurement.

IV. Quantum vs classical inception score

Here, we compare the qIS with its classical counterpart. By introducing projective measurements, we can recover the cIS as follow. To classify the data into ℓ labels, we assume $\ell = d' = \dim(\mathcal{H}'_S)$. Let $\{|y_j\rangle\}_{j=0}^{\ell-1}$ be an orthonormal basis for $\mathcal{H}'_S$. Then, the rank-1 projective measurement onto the orthogonal state $|y_j\rangle$ is given by $\Pi_j \equiv |y_j\rangle\langle y_j|$. Then, we have $\Pi_j\Pi_k = \Pi_j\delta_{jk}$ with δ_{jk} the Kronecker's delta. Also, the completeness relation $\sum_{j=0}^{\ell-1}\Pi_j = \mathbb{1}$ holds, where $\mathbb{1}$ denotes the identity operator acting on $\mathcal{H}'_S$. Regarding the dimensions of the Hilbert spaces, hence, the meaningful setup is $d \geqslant r \geqslant \ell$. Therefore, Φ belongs to the class of tree-like quantum classifiers composed of the hierarchical quantum circuits [45, 46, 56–59], where the compressed states are expected to carry the features of the encoded data $\mathcal{X}$.

For a state $\rho \in \mathcal{B}(\mathcal{H}'_S)$, let us write the post-projection-measurement state as

$$\mathcal{P}(\rho) \equiv \sum_{j=0}^{\ell-1}\Pi_j\rho\Pi_j = \sum_{j=0}^{\ell-1}\langle y_j|\rho|y_j\rangle|y_j\rangle\langle y_j| , \tag{13}$$

which is also a dephasing map generating an incoherent state diagonal in the basis $\{|y_j\rangle\}_{j=0}^{\ell-1}$. Then, the probability that the output state takes $|y_j\rangle$ is given by $p(y_j) \equiv \mathrm{Tr}[\rho_{\rm out}\Pi_j] = \langle y_j|\rho_{\rm out}|y_j\rangle$. From Eqs. (3), (4), and (5), we have $p(y_j|x_i) \equiv \mathrm{Tr}[\rho_{\rm out}^{(i)}\Pi_j] = \langle y_j|\rho_{\rm out}^{(i)}|y_j\rangle$. Because $\mathcal{P}(\rho_{\rm out}^{(i)})$ and $\mathcal{P}(\rho_{\rm out})$ have the identical eigenbasis $\{|y_j\rangle\}_{j=0}^{\ell-1}$, we have $S(\mathcal{P}(\rho_{\rm out}^{(i)})\,\|\,\mathcal{P}(\rho_{\rm out})) = D(p(y|x_i)\,\|\,p(y))$, meaning that the cIS in Eq. (1) can be recovered from Eq. (11) by projective measurements.

Therefore, writing the Holevo information of the projected output ensemble due to $\mathcal{P}$ as

$$\chi_{\mathcal{P}}(\mathcal{E};\rho_{\rm out}) \equiv \sum_{i=0}^{r-1}p(x_i)S(\mathcal{P}(\rho_{\rm out}^{(i)})\,\|\,\mathcal{P}(\rho_{\rm out})) , \tag{14}$$

we can define the cIS dependent on the choice of $\mathcal{P}$ as

$$\xi_c(\mathcal{P}) \equiv \exp\left(\chi_{\mathcal{P}}(\mathcal{E};\rho_{\rm out})\right) . \tag{15}$$

Extending to the positive operator-valued measures (POVMs) $\mathcal{M} \equiv \{E_j\}_{j=0}^{\ell-1}$, where $E_j \geqslant 0$ is a POVM element satisfying $\sum_{j=0}^{\ell-1}E_j = \mathbb{1}$. Also, note that with jth POVM element, the probabilities are $p(y_j) \equiv \mathrm{Tr}[\rho_{\rm out}E_j]$ and $p(y_j|x_i) \equiv \mathrm{Tr}[\rho_{\rm out}^{(i)}E_j]$. The maximum cIS can be given by the *accessible information* [37, 60–63]

$$\begin{aligned} I_{\rm acc}&(\mathcal{E};\rho_{\rm out}) \\ &\equiv \max_{\{\mathcal{M}\}}\left[\sum_{j=0}^{\ell-1}\sum_{i=0}^{r-1}p(x_i)\mathrm{Tr}[\rho_{\rm out}^{(i)}E_j]\ln\mathrm{Tr}[\rho_{\rm out}^{(i)}E_j]\right. \\ &\qquad\left. - \sum_{j=0}^{\ell-1}\mathrm{Tr}[\rho_{\rm out}E_j]\ln\mathrm{Tr}[\rho_{\rm out}E_j]\right] \\ &= \max_{\{\mathcal{M}\}}\left[\sum_{i=0}^{r-1}p(x_i)D_{\mathcal{M}}(p(y|x_i)\,\|\,p(y))\right] , \end{aligned} \tag{16}$$

which is the maximization of the classical mutual information over all possible POVMs $\{\mathcal{M}\}$. Here, we intentionally write $D_{\mathcal{M}}$ to emphasize the dependence of the KL divergence on the choice of the POVMs. The Holevo theorem states [37]

$$\chi(\mathcal{E};\rho_{\rm out}) \geqslant I_{\rm acc}(\mathcal{E};\rho_{\rm out}) \tag{17}$$

with the equality if and only if

$$[\rho_{\rm out}^{(n)}, \rho_{\rm out}^{(m)}] = 0 \ (\forall n, \forall m) , \tag{18}$$

implying that $\rho_{\rm out}^{(n)}$ and $\rho_{\rm out}^{(m)}$ can be simultaneously diagonalized.

By defining the *accessible IS* as

$$\xi_{\rm acc} \equiv \exp(I_{\rm acc}(\mathcal{E};\rho_{\rm out})) , \tag{19}$$

we can obtain our second main result as follows

Theorem 1. *The inception scores, ξ_q, $\xi_{\rm acc}$, and $\xi_c(\mathcal{P})$, satisfy*

$$\ell \geqslant \xi_q \geqslant \xi_{\rm acc} \geqslant \xi_c(\mathcal{P}) \ (\forall\mathcal{P}) . \tag{20}$$

Proof. First, $\xi_q \geqslant \xi_{\rm acc}$ is the Holevo theorem itself. Second, because the projective measurements belong to the POVMs, from Eq. (16), we must have $\xi_{\rm acc} \geqslant \xi_c(\mathcal{P})$. Finally, from $\ln(\ell) \geqslant \chi(\mathcal{E};\rho_{\rm out})$ and Eq. (11), we have $\ell \geqslant \xi_q$. Therefore, we can obtain Eq. (20). □

Theorem 1 implies that the quantum generative model has better quality than its classical counterpart.

V. Quantum coherence and quality

From Thm. 1, it is natural to ask what is the quantum resource for this advantage. The answer to this question is the quantum coherence. In the following, we demonstrate that the quantum coherence preserved during the classification process is the resource to enable the quantum generative models to have better quality than their classical counterparts.

A. Review of resource theory of asymmetry

First, we briefly review the resource theory of asymmetry (RTA) [64–77], where the quantum coherence is regarded as a resource of breaking the group symmetry. Let G be a symmetry group, and g be the group element with its unitary representation $U_g : G \to \mathcal{B}(\mathcal{H})$ acting on a D-dimensional Hilbert space $\mathcal{H}$. Let

$$\mathcal{I}_G(\mathcal{H}) \equiv \{\sigma \,|\, U_g \sigma U_g^\dagger = \sigma, \forall g \in G, \sigma \in \mathcal{B}(\mathcal{H})\} \tag{21}$$

be the set of the free states in the RTA, which are invariant under any unitary operations with respect to g. The free state satisfies the commutation relation $[\rho, U_g] = 0$ $(\forall g)$ and is called the *symmetric* state with respect to G, and *asymmetric* state otherwise, which becomes a resource state in the RTA.

A relevant set of free operations are the covariant operations Λ [78] with respect to G, which satisfies

$$\Lambda(U_g \rho U_g^\dagger) = U_g \Lambda(\rho) U_g^\dagger \;\; (\forall g \in G, \forall \rho \in \mathcal{B}(\mathcal{H}))\,. \tag{22}$$

The covariant operation cannot generate the asymmetric states from the symmetric state and transform one asymmetric state to the other.

To quantify the asymmetry of a given quantum state ρ with respect to G, a asymmetry measure $A(\rho;G)$ needs to satisfy the following conditions: The asymmetry measure must satisfy

1. $A(\rho;G) \geqslant 0$ $(\forall \rho \in \mathcal{B}(\mathcal{H}))$ and $A(\rho;G) = 0 \Longleftrightarrow \rho \in \mathcal{I}_G(\mathcal{H})$.

2. For all covariant operations $\{\Lambda\}$, we must have $A(\rho;G) \geqslant A(\Lambda(\rho);G)$ $(\forall \rho \in \mathcal{B}(\mathcal{H}))$.

One of the asymmetry measures is the *relative entropy of asymmetry* [75]. To define the relative entropy of asymmetry, let us first introduce the G-twirling operation [72–78], which is defined as

$$\mathcal{G}(\rho) \equiv \int_G dg U_g \rho U_g^\dagger \tag{23}$$

averaging over the unitary operations with the Haar measure dg [79]. When G is a finite or compact Lie group, the relative entropy of asymmetry with respect to G is defined as [75]

$$A(\rho;G) \equiv S(\rho \,\|\, \mathcal{G}(\rho))\,. \tag{24}$$

Now, let us consider the case $G = U(1)$ generated by an observable H, whose unitary representations form a set of time translations $\{e^{-itH} \,|\, \forall t \in \mathbb{R}\}$. In this case, ρ is a symmetric state if and only if $[\rho, H] = 0$ and an asymmetric state if and only if $[\rho, H] \neq 0$ [70]. Therefore, when ρ is a symmetric state, ρ can be diagonalized by the eigenbasis of H. Let us write $A(\rho;H)$ as the relative entropy of asymmetry for this case. When H has L distinct eigenvalues, the explicit form of the corresponding $U(1)$-twirling operation with respect to H is given by [75, 76] (see Appendix. A for detailed explanations)

$$\mathcal{G}_H(\rho) \equiv \lim_{T\to\infty}\left[\frac{1}{2T}\int_{-T}^{T} dt e^{-iHt} \rho e^{iHt}\right] = \sum_{n=1}^{L} \Pi_n \rho \Pi_n, \tag{25}$$

where $L \leqslant D$ and $\{\Pi_n\}_{n=1}^L$ are the projectors onto the subspace of the eigenbasis of H. Then, the relative entropy of asymmetry $A(\rho, H) \equiv S(\rho \,\|\, \mathcal{G}_H(\rho))$ coincides with the so-called relative entropy of superposition with respect to the orthogonal decomposition of the Hilbert space [80]. Particularly, when H is nondegenerate (i.e. $L = D$), we have $\mathrm{rank}(\Pi_n) = 1$ $(\forall n)$, and the relative entropy of asymmetry coincides with the relative entropy of coherence with respect to the eigenabsis of H [81].

B. Asymmetry and quantum inception score

Now, we are ready to discuss the relation between the quantum inception score and the quantum coherence captured by the asymmetry with respect to $U(1)$ group generated by $\rho_{\rm out}^{(i)}$ the constituent states of the output state.

For the output state $\rho_{\rm out} = \sum_{i=0}^{r-1} p(x_i)\rho_{\rm out}^{(i)}$ with its fixed ensemble $\mathcal{E} = \{p(x_i), \rho_{\rm out}^{(i)}\}_{i=0}^{r-1}$, for each i, we consider the set of time translations $\{e^{-i\rho_{\rm out}^{(i)} t} \,|\, \forall t \in \mathbb{R}\}$. When $[\rho_{\rm out}^{(n)}, \rho_{\rm out}^{(m)}] = 0$ $(\forall n, \forall m)$, we particularly call the corresponding ensemble as *symmetric ensemble*

$$\mathcal{E}_S \equiv \left\{p(x_i), \rho_{\rm out}^{(i)} \,\middle|\, [\rho_{\rm out}^{(n)}, \rho_{\rm out}^{(m)}] = 0 \; (\forall n, \forall m)\right\}_{i=0}^{r-1}. \tag{26}$$

On the other hand, we define the *asymmetric ensemble* as

$$\overline{\mathcal{E}_S} \equiv \left\{p(x_i), \rho_{\rm out}^{(i)} \,\middle|\, [\rho_{\rm out}^{(n)}, \rho_{\rm out}^{(m)}] \neq 0 \; (\exists n, \exists m)\right\}_{i=0}^{r-1}, \tag{27}$$

which is the complement of $\mathcal{E}_S$. To explore the relation between the quantum inception score and the asymmetry measure, we define the average relative entropy of asymmetry of the output state $\rho_{\rm out}$ as

$$\langle A(\rho_{\rm out}; H)\rangle \equiv \sum_{i=0}^{r-1} p(x_i) A(\rho_{\rm out}^{(i)}; H)\,, \tag{28}$$

which measures the average amount of coherence contained by $\rho_{\rm out}$, which is characterized by the asymmetry with respect to the $U(1)$ group generated contained by H. Then, we can obtain our *third main result* as follows

Theorem 2. *For the output state $\rho_{\rm out} = \sum_{i=0}^{r-1} p(x_i)\rho_{\rm out}^{(i)}$ with its fixed ensemble $\mathcal{E} = \{p(x_i), \rho_{\rm out}^{(i)}\}_{i=0}^{r-1}$, we have*

$$\xi_q > \xi_{\rm acc} \Longleftrightarrow \mathcal{E} = \overline{\mathcal{E}_S} \Longleftrightarrow \langle A(\rho_{\rm out}; \rho_{\rm out}^{(k)})\rangle \neq 0 \ (\exists k)\,. \tag{29}$$

Proof. We prove by taking the contraposition of the following statement

$$\xi_q = \xi_{\rm acc} \Longleftrightarrow \mathcal{E} = \mathcal{E}_S \Longleftrightarrow \langle A(\rho_{\rm out}; \rho_{\rm out}^{(k)})\rangle = 0 \ (\forall k)\,. \tag{30}$$

For the first part, $\xi_q = \xi_{\rm acc} \Longleftrightarrow \mathcal{E} = \mathcal{E}_S$ is the Holevo theorem.

For the second part, We consider a set of time translations $\{e^{-it\rho_{\rm out}^{(k)}} \,|\, \forall t \in \mathbb{R}\}$ generated by the density operator of the constituent state $\rho_{\rm out}^{(k)}$.

Let us prove the sufficiency. When $\mathcal{E} = \mathcal{E}_S$, we have $[\rho_{\rm out}^{(i)}, \rho_{\rm out}^{(k)}] = 0 \ (\forall i, \forall k)$. Therefore, the relative entropy of asymmetry of $\rho_{\rm out}^{(i)}$ with respect to $\rho_{\rm out}^{(k)}$ must vanish, i.e. $A(\rho_{\rm out}^{(i)}; \rho_{\rm out}^{(k)}) = 0 \ (\forall i, \forall k)$, because of the condition of the asymmetry measure. Therefore, from Eq. (28), we have $\langle A(\rho_{\rm out}; \rho_{\rm out}^{(k)})\rangle = 0 \ (\forall k)$. Therefore, the sufficiency holds

$$\mathcal{E} = \mathcal{E}_S \Longrightarrow \langle A(\rho_{\rm out}; \rho_{\rm out}^{(k)})\rangle = 0 \ (\forall k)\,. \tag{31}$$

Next, let us prove the necessity. Let us focus on Eq. (28). Here, we have $p(x_i) > 0 \ (\forall i)$ and the nonnagativity of the quantum relative entropy $S(\rho_{\rm out}^{(i)} \,\|\, \mathcal{G}_k(\rho_{\rm out}^{(i)})) \geqslant 0 \ (\forall i, \forall k)$, where $\mathcal{G}_k$ denotes the $U(1)$-twirling operation with respect to $\rho_{\rm out}^{(k)}$. Therefore, when we have $\langle A(\rho_{\rm out}; \rho_{\rm out}^{(k)})\rangle = 0 \ (\forall k)$, we must have $S(\rho_{\rm out}^{(i)} \,\|\, \mathcal{G}_k(\rho_{\rm out}^{(i)})) = 0 \ (\forall i, \forall k)$. From the condition of the asymmetry measure, this implies $[\rho_{\rm out}^{(i)}, \rho_{\rm out}^{(k)}] = 0 \ (\forall i, \forall k)$, namely $\mathcal{E} = \mathcal{E}_S$. Therefore, the necessity holds:

$$\langle A(\rho_{\rm out}; \rho_{\rm out}^{(k)})\rangle = 0 \ (\forall k) \Longrightarrow \mathcal{E} = \mathcal{E}_S\,. \tag{32}$$

From Eqs. (31) and (32), we can obtain Eq. (30). By taking its contraposition, we obtain Eq. (29), which proves Thm. 2. □

This theorem demonstrates that the qIS is larger than its classical counterpart if and only if $\rho_{\rm out}$ has an asymmetry with respect to the $U(1)$ group generated by some constituent states $\rho_{\rm out}^{(i)}$. This means that the quantum coherence preserved during the classification process, captured by the asymmetry, is the resource for the quantum generative model to have better quality than its classical counterpart. Also, note that this theorem holds for any asymmetry measures, such as skew informations [68–71].

VI. Physical limitation

Finally, we discuss the physical limitation of the quality of quantum generative models. From Thm. 2, we can also expect that the pure dephasing (or decoherence) contributes to degrading the quality into the classical one. Here, we analyze this observation in a quantitative way by employing the information-theoretic fluctuation theorems [40–42] based on the concept of the quantum efficacy [42–44]. Following Ref. [42], when Δa is a random variable whose average is $\langle \Delta a\rangle = \chi(\mathcal{E}; \rho_{\rm out}) - \chi_{\mathcal{P}}(\mathcal{E}; \rho_{\rm out})$, the corresponding quantum fluctuation theorem is given as $\langle \exp(-\Delta a)\rangle = \gamma$, where γ is called quantum efficacy [82] and satisfies $0 < \gamma \leqslant 1$.

From the Jensen's inequality, we have $\chi(\mathcal{E}; \rho_{\rm out}) - \chi_{\mathcal{P}}(\mathcal{E}; \rho_{\rm out}) \geqslant -\ln\gamma$. Here, note that γ is strictly dependent on Φ and the choice of the projective measurement $\mathcal{P}$. Then, we can obtain our *fourth main result* as follows.

Theorem 3. *The quantum inception score can be lower bounded by using quantum efficacy γ as*

$$\xi_q \geqslant \frac{\xi_c(\mathcal{P})}{\gamma} \quad (0 < \gamma \leqslant 1)\,. \tag{33}$$

Proof. By definitions, we have $\xi_q \equiv \exp(\chi(\mathcal{E}; \rho_{\rm out}))$ and $\xi_c(\mathcal{P}) \equiv \exp(\chi_{\mathcal{P}}(\mathcal{E}; \rho_{\rm out}))$. Because $\exp(-\ln\gamma) = \gamma^{-1}$, we can obtain $\xi_q \geqslant \gamma^{-1}\xi_c(\mathcal{P})$ with $0 < \gamma \leqslant 1$. □

From Refs. [42, 83], when $\gamma = 1$, the equality of Eq. (33) holds if and only if all $\rho_{\rm out}^{(i)}$ have *identical* eigenbasis and $\mathcal{P}$ is the dephasing map onto this common eigenbasis, i.e. $\mathcal{P}(\rho_{\rm out}^{(i)}) = \rho_{\rm out}^{(i)} \ (\forall i)$. Therefore, we have $\rho_{\rm out} = \mathcal{P}(\rho_{\rm out})$, which means that $\rho_{\rm out}$ is an incoherent state diagonal in this common eigenbasis. This implies that the quality degradation of the quantum generative model is primarily due to the pure dephasing process. This analysis also enables us to interpret γ as a quantity characterizing the *physical limitation* of the quality due to the information loss. In particular, the negative logarithm $(-\ln\gamma)$ accounts for the information content contained by the quantum coherence, which is preserved during the classification process.

VII. Application to a phase classification problem in quantum many-body physics

As an example, we harness the quantum inception score to analyze the quality of a fixed quantum generator with a trainable quantum classifier. Here, the generator is the one-dimensional (1D) spin-1/2 chain that may experience phase transition, and the classifier is the quantum convolutional neural network (QCNN) [45].

A. QCNNs

The architecture of the QCNNs were introduced in Refs. [45, 46], which are expected to be promising near-term quantum algorithms as quantum classifiers [56–59] because of their absence of barren plateaus [84] resulting in the trainability of the QCNNs [85–89]. Following Ref. [84], let us consider the following QCNN circuit (see Fig. 2 as an example for the 8-qubit case).

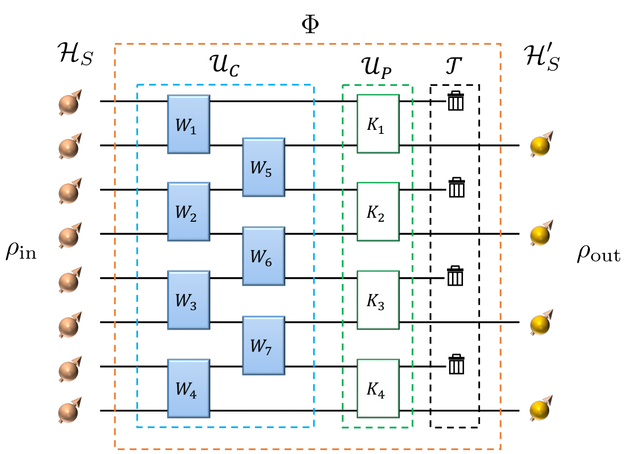

FIG. 2. 8-qubit Quantum Convolutional Neural Network. $\mathcal{U}_C$ and $\mathcal{U}_P$ denote the convolutional and pooling layer. $\{W_1, \cdots, W_7\}$ are the 2-qubit unitaries acting on the pairs of qubits in an alternating manner, which are parameterized by some tunable parameters. $\{K_1, \cdots, K_4\}$ are the 2-qubit unitaries with the form of $K_j \equiv |0\rangle\langle 0| \otimes U_j + |1\rangle\langle 1| \otimes V_j$, where U_j and V_j are single-qubit unitaries parameterized by some tunable parameters. $\mathcal{T} \equiv \mathrm{Tr}_{\overline{\mathcal{H}}'_S}$ denotes the partial trace over $\overline{\mathcal{H}}'_S$ (the complement of $\mathcal{H}'_S$). Then, the quantum classifier channel is given by $\Phi \equiv \mathcal{T} \circ \mathcal{U}_P \circ \mathcal{U}_C$.

The input state ρ_{in} is an N-qubit state, which may encode the classical data, namely the output of a generator. Then, we send ρ_{in} into the single layered convolutional circuit denoted by a unitary operation $\mathcal{U}_C$ and then the pooling circuit denoted by another unitary operation $\mathcal{U}_P$. The convolutional circuit $\mathcal{U}_C$ consists of two columns of the alternating 2-qubit gate parameterized by some tunable parameters. The pooling circuit $\mathcal{U}_P$ consists of the 2-qubit gates with the form of $K_j = |0\rangle\langle 0| \otimes U_j + |1\rangle\langle 1| \otimes V_j$, where j denotes the jth pair of the qubits, and U_j and V_j are single-qubit gates parameterized by some tunable parameters. Then, we take the partial trace $\mathcal{T} \equiv \mathrm{Tr}_{\overline{\mathcal{H}}'_S}$ over $\overline{\mathcal{H}}'_S$, the complement of the output Hilbert space $\mathcal{H}'_S$, to obtain the output state ρ_{out}. Therefore, the whole process is written as

$$\rho_{\text{out}} = \Phi(\rho_{\text{in}}) \equiv \mathcal{T} \circ \mathcal{U}_P \circ \mathcal{U}_C(\rho_{\text{in}}) . \tag{34}$$

B. Setup and problem formulation

1. Generator and quantum dataset

Adopting the same model studied in Ref. [45], we employ the QCNN to classify 2-class and 3-class quantum phases. The target quantum state to be classified, $\rho_{\text{in}}(x) = |\psi_0(x)\rangle\langle\psi_0(x)|$, is the ground state of an N-body Hamiltonian of a 1D spin-1/2 chain with open boundary conditions [90, 91]:

$$H = -J\sum_{n=1}^{N-2} Z_n X_{n+1} Z_{n+2} - h_1 \sum_{n=1}^{N} X_n - h_2 \sum_{n=1}^{N-1} X_n X_{n+1}, \tag{35}$$

where $\{X_n, Y_n, Z_n\}$ are the Pauli matrices of the nth spin. Also, J, h_1, and h_2 are the strength of the cluster coupling, the global transverse field, and the nearest-neighboring Ising coupling, respectively. These parameters take several values, which accordingly lead to several ground states of H. In particular, we collect those parameters into the vector

$$x \equiv \begin{pmatrix} h_1/J \\ h_2/J \end{pmatrix} \tag{36}$$

and we write the corresponding Hamiltonian in Eq. (35) as $H(x)$.

Here, we consider the case of $N = 9$. The parameters h_1/J and h_2/J take equally separated 64 values in the intervals $h_1/J \in [0, 1.6]$ and $h_2/J \in [-1.6, 1.6]$, respectively; therefore, we consider totally $64 \times 64 = 4096$ points, i.e. $\{x_i\}_{i=0}^{4095} = \{\boldsymbol{z}_{n,m}\}_{(n,m)=(0,0)}^{(63,63)}$ where

$$\boldsymbol{z}_{n,m} \equiv \begin{pmatrix} \frac{1.6}{63} n \\ -1.6 + \frac{3.2}{63} m \end{pmatrix} \ (n, m = 0, 1, \cdots, 63) . \tag{37}$$

Later, we will show the phase diagram of the ground states $\{\rho_{\text{in}}(x_i)\}_{i=0}^{4095}$.

Apart from these parameter points, we take 40 ground states $\{\rho_{\text{in}}(x_i)\}_{i=0}^{39}$ as the training quantum data, where the parameter vectors $\{x_0, x_1, \cdots, x_{39}\}$ are taken as $h_1/J = 1$ and $h_2/J \in [-1.6, 1.6]$, namely

$$x_i \equiv \begin{pmatrix} 1 \\ -1.6 + \frac{3.2}{39} i \end{pmatrix} \ (i = 0, 1, \cdots, 39) . \tag{38}$$

In our simulation, the ground state $\rho_{\text{in}}(x_i)$ is obtained by diagonalizing $H(x_i)$.

(a) 2-class phase classification		
Label	h_2/J	Phase
0	$-1.15 < h_2/J < 0$	SPT
1	$h_2/J < -1.15$ or $h_2/J > 0$	Other phases
(b) 3-class phase classification		
Label	h_2/J	Phase
0	$-1.15 < h_2/J < 0$	SPT
1	N/A	Nothing
2	$h_2/J > 0$	Paramagnetic
3	$h_2/J < -1.15$	Antiferromagnetic

TABLE I. The (a) 2-class and (b) 3-class phase of the ground state of the Hamiltonian (35) when $h_1/J = 1$. Note that for the 3-class case, we employ a 4-valued POVM, and the label "1" has the meaning of "fail in classification".

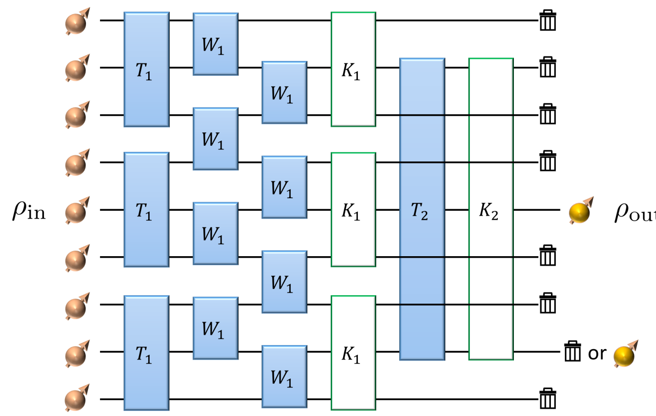

FIG. 3. The 9-qubit QCNN circuit for the 2-class and 3-class quantum phase classification problems. T_j and K_j denote the 3-qubit gate, and W_j denotes the 2-qubit gate. We take partial trace over all qubits except for the 5th qubit for 2-class and except for both the 5th and 8th qubits for the 3-class classification, respectively.

Table I summarizes the labels (the phase) for the 2-class and 3-class cases when $h_1/J = 1$. For the 2-class classification problem, we assign the label "0" to the $\mathbb{Z}_2 \times \mathbb{Z}_2$ symmetry-protected topological (SPT) phase [92–94] when $-1.15 < h_2/J < 0$ and "1" to the other phases. For the 3-class classification problem, we assign the label "0" to the SPT phase when $-1.15 < h_2/J < 0$, "2" to the paramagnetic phase when $h_2/J > 0$, and "3" to the antiferromagnetic phase when $h_2/J < -1.15$. Note that, later in the discussion, we introduce a 4-valued POVM to classify the phase, where the additional label "1" has the meaning of "fail in classification". Also, the general phase other than the case $h_1/J = 1$ will be shown later.

2. *Training of QCNN*

The QCNN circuit used for this quantum phase classification problem is shown in Fig. 3. This circuit consists of $N = 9$ qubits, and it contains 117 learning parameters for the 2-class classification and 156 for the 3-class classification problems, respectively. The gates with the same name and index share the same parameters. The convolutional layer consists of W_j and T_j. W_j is the 2-qubit convolutional gate with the form of $W_j = (V \otimes V)e^{-i\boldsymbol{\theta}\cdot(ZZ,YY,XX)}(V \otimes V)$, where $\boldsymbol{\theta}$ is the 3-dimensional vector and V is the single-qubit gate with the form of $V = e^{-i\phi_1 Z}e^{-i\phi_2 Y}e^{-i\phi_3 X}$ which has 3 parameters. W_j has 15 parameters since each V in W_j has different parameters. T_j is the 3-qubit convolutional gate with the form of $T_j = W^{(3,1)}W^{(2,3)}W^{(1,2)}$, where $W^{(a,b)}$ acts on qubits indexed by a and b. T_j has 45 parameters since each W in T_j has different paramters. The pooling layer consists of K_j. For the 2-class classification, K_j is the 3-qubit pooling gate with the form of $K_j = (\mathbb{1}\otimes\mathbb{1}\otimes|0\rangle\langle 0|+\mathbb{1}\otimes V\otimes|1\rangle\langle 1|)(|0\rangle\langle 0|\otimes\mathbb{1}\otimes\mathbb{1}+|1\rangle\langle 1|\otimes V\otimes\mathbb{1})$ which has 6 parameters. For the 3-class classification, K_1 is the same as K_j described above, while K_2 is the same form as T_j.

As for the dimensions of the Hilbert space of the output state, we have $\ell = 2$ for the 2-class classification and $\ell = 4$ for the 3-class classification problems, respectively. This corresponds to the partial trace operation after applying K_2; that is, we take the partial trace over all qubits except for the 5-th qubit for the 2-class classification and except for both 5-th and 8-th qubits for the 3-class classification, respectively. Let us define $|+\rangle$ and $|-\rangle$ as $|\pm\rangle \equiv (|0\rangle \pm |1\rangle)/\sqrt{2}$, where $\{|0\rangle, |1\rangle\}$ is the computational basis. Then, for the 2-class classification, we define $\Pi_0 \equiv |+\rangle\langle +|$ and $\Pi_1 \equiv |-\rangle\langle -|$ as the projectors corresponding to the labels "0" and "1", respectively. For the 3-class classification, we define $\Pi_0 \equiv |+,+\rangle\langle +,+|$, $\Pi_1 \equiv |+,-\rangle\langle +,-|$, $\Pi_2 \equiv |-,+\rangle\langle -,+|$ and $\Pi_3 \equiv |-,-\rangle\langle -,-|$ as the projectors corresponding to the labels "0", "1", "2" and "3", respectively.

In the QCNN training procedure, we minimize the cost function by updating the parameters of QCNN with the use of the Simultaneous Perturbation Stochastic Approximation (SPSA) optimizer [95, 96]. Here, the cost function is the cross-entropy loss given by

$$\begin{aligned}\mathcal{L}(\Phi) &= -\sum_{i,j} p_{\text{true}}(x_i, y_j) \ln p_{\text{train}}(x_i, y_j) \\ &= -\sum_{i,j} p_{\text{true}}(y_j|x_i)p(x_i) \ln(p_{\text{train}}(y_j|x_i)p(x_i)) \\ &= -\frac{1}{r}\sum_{i,j} p_{\text{true}}(y_j|x_i) \ln \frac{p_{\text{train}}(y_j|x_i)}{r} \\ &= -\frac{1}{r}\sum_{i,j} p_{\text{true}}(y_j|x_i) \ln p_{\text{train}}(y_j|x_i) + \ln r,\end{aligned} \tag{39}$$

where

$$p_{\text{train}}(y_j|x_i) \equiv \mathrm{Tr}\left[\Phi(\rho_{\text{in}}(x_i))\Pi_j(x_i)\right], \tag{40}$$

with Φ the QCNN and $\Pi_j(x_i)$ the projector corresponding to the label y_j of the training data x_i encoded in

$\rho_{\rm in}(x_i)$. Also, $p_{\rm true}(y_j|x_i)$ is the true distribution, where y_j is the index of phase assigned to $\rho_{\rm in}(x_i)$. Recall that we are given 40 training data (38), and we here assume that $\rho_{\rm in}(x_i)$ appears with equal probability $p(x_i) = 1/40$.

3. Prediction and quality evaluation

After training the QCNN, we apply the trained QCNN to predict the phase (label) of test data [97] and then compute the qIS and cIS, for the 2-class and 3-class classifications problems in the following two scenarios. The first is the unbiased scenario where we randomly generate equal numbers of data for every label, and the second is the biased scenario where the numbers of randomly generated data are (largely) different for each label. Clearly, the former has a bigger diversity in the data, or equivalently the generator has a capability to produce a bigger variety of data; thus the values of both qIS and cIS for the former case would be bigger compared to the latter case.

In the simulation, the total number of test data is $r = 1500$, where the labels are given as follows. For the 2-class classification problem, in the unbiased case we randomly select 750 data with label "0" and 750 data with label "1"; in the biased case we randomly select 1480 data with label "0" and 20 data with label "1". For the 3-class classification problem, in the unbiased case we randomly select 500 data with label "0", 500 data with "2", and 500 data with "3"; in the biased case we randomly select 1480 data with label "0", 10 data with "2" and 10 data with "3". Table II shows the summary of the setting described above. In all cases, each data is generated with equal probability; that is, we suppose

$$p(x_i) = \frac{1}{1500}\ (\forall i)\,. \tag{41}$$

(a) 2-class phase classification		
Label	unbiased	biased
0	750	1480
1	750	20
(b) 3-class phase classification		
Label	unbiased	biased
0	500	1480
1	0	0
2	500	10
3	500	10

TABLE II. Number of randomly selected test data for the (a) 2-class and (b) 3-class classification problems.

With the above setting, we can compute qIS simply using Eqs. (7) and (11) with $r = 1500$. To compute the cIS $\xi_c(\mathcal{P})$, we further need to specify the measurement or equivalently the measurement process $\mathcal{P}$. In our simulation, for the 2-class classification problem, we take the following dephasing operations:

$$\mathcal{P}_2(\rho) \equiv \langle +|\rho|+\rangle |+\rangle\langle +| + \langle -|\rho|-\rangle |-\rangle\langle -|. \tag{42}$$

Also, for the 3-class classification problems, we take

$$\begin{aligned}\mathcal{P}_3(\rho) \equiv\ & \langle +,+|\rho|+,+\rangle |+,+\rangle\langle +,+| \\ &+ \langle +,-|\rho|+,-\rangle |+,-\rangle\langle +,-| \\ &+ \langle -,+|\rho|-,+\rangle |-,+\rangle\langle -,+| \\ &+ \langle -,-|\rho|-,-\rangle |-,-\rangle\langle -,-|\,.\end{aligned} \tag{43}$$

Furthermore, we consider the problem of calculating the accessible information $I_{\rm acc}$ given by Eq. (16) for the 2-class classification problem. In particular, instead of maximizing $\{\mathcal{M}\}$ over all possible POVMs, we here consider an optimization problem of the projectors in the following form:

$$\begin{aligned}\Pi_0(\theta,\phi) &\equiv |\psi_0(\theta,\phi)\rangle\langle\psi_0(\theta,\phi)|, \\ \Pi_1(\theta,\phi) &\equiv |\psi_1(\theta,\phi)\rangle\langle\psi_1(\theta,\phi)|\,,\end{aligned} \tag{44}$$

where

$$\begin{aligned}\psi_0(\theta,\phi) &\equiv \cos(\theta/2)|0\rangle + e^{i\phi}\sin(\theta/2)|1\rangle, \\ \psi_1(\theta,\phi) &\equiv \sin(\theta/2)|0\rangle - e^{i\phi}\cos(\theta/2)|1\rangle\,.\end{aligned} \tag{45}$$

That is, we optimize the parameters (θ, ϕ) so that the cIS is maximized.

For the 3-class classification problem, we use the projectors in the following form:

$$\begin{aligned}\Pi_0(\boldsymbol{\theta}) &\equiv U(\boldsymbol{\theta})|0,0\rangle\langle 0,0|U^\dagger(\boldsymbol{\theta})\,, \\ \Pi_1(\boldsymbol{\theta}) &\equiv U(\boldsymbol{\theta})|0,1\rangle\langle 0,1|U^\dagger(\boldsymbol{\theta})\,, \\ \Pi_2(\boldsymbol{\theta}) &\equiv U(\boldsymbol{\theta})|1,0\rangle\langle 1,0|U^\dagger(\boldsymbol{\theta})\,, \\ \Pi_3(\boldsymbol{\theta}) &\equiv U(\boldsymbol{\theta})|1,1\rangle\langle 1,1|U^\dagger(\boldsymbol{\theta})\,,\end{aligned} \tag{46}$$

where $\boldsymbol{\theta}$ is the 15-dimensional vector and

$$\begin{aligned}U(\boldsymbol{\theta}) \equiv\ & (e^{-i\theta_1 Z}e^{-i\theta_2 Y}e^{-i\theta_3 X} \otimes e^{-i\theta_4 Z}e^{-i\theta_5 Y}e^{-i\theta_6 X}) \\ & \times e^{-i(\theta_7 ZZ + \theta_8 YY + \theta_9 XX)} \\ & \times (e^{-i\theta_{10} Z}e^{-i\theta_{11} Y}e^{-i\theta_{12} X} \otimes e^{-i\theta_{13} Z}e^{-i\theta_{14} Y}e^{-i\theta_{15} X})\,.\end{aligned} \tag{47}$$

C. Simulation results

The inception scores for the 2-class and 3-class phase classifications are shown in Table III. In the 2-class case, we calculate ξ_c with the projection measurement on the X-axis and Z-axis, which correspond to $(\theta, \phi) = (\pi/2, 0)$ and $(\theta, \phi) = (0, \pi)$ in Eq. (44), respectively. Also, we calculate ξ_c with the high-accuracy-axis; that is, (θ, ϕ) are chosen so that the classification accuracy, which is the ratio of the number of matches between the predicted labels and the correct labels to that of all data $\{x_i\}_{i=0}^{4095}$, is almost maximized. Moreover, we calculate ξ_c with the optimized-axis, meaning that we choose (θ, ϕ) that maximizes cIS. In the 3-class case, ξ_c with the XX-axis and the ZZ-axis are calculated by the projectors $\{|+,+\rangle\langle+,+|, |+,-\rangle\langle+,-|, |-,+\rangle\langle-,+|, |-,-\rangle\langle-,-|\}$ and $\{|0,0\rangle\langle0,0|, |0,1\rangle\langle0,1|, |1,0\rangle\langle1,0|, |1,1\rangle\langle1,1|\}$, respectively. For the high-accuracy-axis, we choose $\boldsymbol{\theta}$ in Eq. (46) so that the classification accuracy is almost maximized. For the optimized-axis, we choose $\boldsymbol{\theta}$ that maximizes cIS. As expected, the qIS of the unbiased case (more diverse case) is larger than that of the biased case; interestingly, the bias-unbias gap for the 3-class case is bigger than that for the 2-class case. Also, the importance of appropriate choice of the measurement is clearly seen; in the 2-class classification for the unbiased case, the normalized error of $\xi_q - \xi_c$ is $(1.123 - 1.111)/2 = 6.0 \times 10^{-3}$, where $\xi_q \leqslant \ell = 2$ is used; also for the 3-class case, the normalized error is $(1.553 - 1.534)/3 \approx 6.3 \times 10^{-3}$.

(a) 2-class phase classification		
Inception Scores	unbiased	biased
ξ_q	1.123	1.028
ξ_c: X-axis	1.095	1.018
ξ_c: Z-axis	1.001	1.001
ξ_c: high-accuracy-axis	1.022	1.005
ξ_c: optimized-axis	1.111	1.023
(b) 3-class phase classification		
Inception Scores	unbiased	biased
ξ_q	1.553	1.126
ξ_c: XX-axis	1.501	1.110
ξ_c: ZZ-axis	1.017	1.006
ξ_c: high-accuracy-axis	1.352	1.073
ξ_c: optimized-axis	1.534	1.115

TABLE III. Inception scores ξ_q and ξ_c for the (a) 2-class and (b) 3-class classification problems. cIS is calculated with several types of projection measurements.

For the 2-class classification problem, we can see the effect of appropriate choice of the measurement axis, using the Bloch sphere representation of the states. Figure 4 shows the plots of the output states of the QCNN in the Bloch sphere, in (a1, a2) the unbiased and (b1, b2) the biased cases. The purple and yellow plots are the output states corresponding to the labels "0" and "1", respectively. The classification task is to design a measurement axis (a single line passing through the origin) for best separating the yellow and purple points. Clearly, a measurement axis on the xy plane better works than the z axis. Next, from the figures (a1,b1), separating the unbiased dataset by a single line on the xy plane seems harder than the case for the biased case. This can be seen in the histogram of the projection results of the QCNN outputs onto the X-axis, shown in Fig. 4 for (a3) the unbiased case and (b3) the biased case, respectively; the horizontal and vertical axes are the expectation value $\langle X\rangle$ of the QCNN output and the number of data belonging to the bin, respectively. That is, in (a3) there is an overlap between the two dataset, while in (b3) the dataset are clearly separated, meaning that the accuracy in the biased case is higher than the unbiased case. However, due to the lack of diversity of the biased dataset, the resulting qIS for the unbiased case takes a higher value than that for the biased one. Apart from these observation, it is interesting that the dataset $\{\rho_{\rm out}(x_i)\}$ construct a near-1D manifold while $\{\rho_{\rm out}(x_i)\}$ is 2D distributed in $(\mathbb{C}^2)^{\otimes 9}$; thus, the classifier (QCNN) Φ works so that the single line (i.e., the measurement axis) could best separate the two dataset.

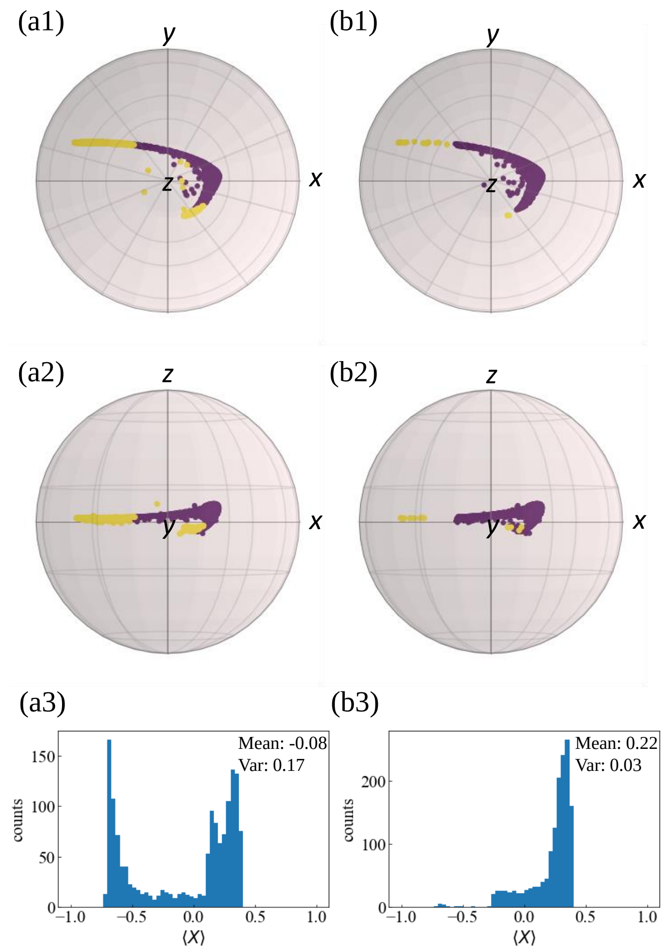

FIG. 4. The Bloch sphere representation and the histograms of the outputs of the QCNN; (a1,a2,a3) show the unbiased case and (b1,b2,b3) show the biased case of the 2-class phase classification problem.

Finally, Fig. 5 shows the phase diagrams predicted by the trained QCNN with the projection measurement onto the (a) X-axis, (b) Z-axis, (c) high-accuracy axis and (d) optimized axis, for the 2-class classification problem; recall that we determined the high-accuracy and optimized axis by appropriately choosing (θ, ϕ) in Eq. (44). Regarding (c) the high-accuracy axis and (d) the optimized axis, we use those obtained in the unbiased case. The ground states of the Hamiltonian (35) are classified to the paramagnetic phase (upper the blue line), the antiferromagnetic phase (below the green line), or the SPT phase between the two lines, where the blue and green lines are the exact phase boundaries obtained by using the infinite size DMRG numerical simulator. The purple and yellow regions correspond to the SPT phase with the label "0" and the paramagnetic/antiferromagnetic phases with the label "1", respectively. That is, for the 2-class case, we do not distinguish the paramagnetic and antiferromagnetic phases. The value of classification accuracy achieved in each measurement methods are: (a) 0.78, (b) 0.49, (c) 0.98, and (d) 0.76. Interestingly, the optimal strategy (d) maximizes ξ_c at the price of not detecting the antiferromagnetic phase, while the QCNN has the ability for detecting that phase as shown in the figure (c). This is consistent to the concept of IS, which quantifies the quality of the generator, defined by the balance between the accuracy and diversity.

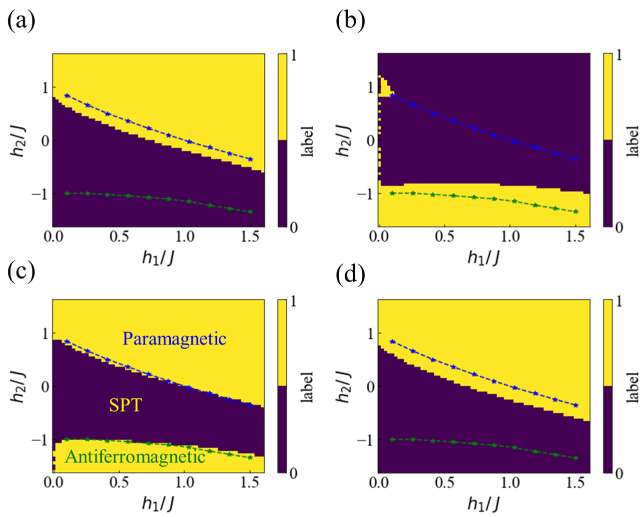

FIG. 5. Phase diagram predicted by the QCNN with the projection measurement onto the (a) X-axis, (b) Z-axis, (c) high-accuracy axis, and (d) optimized axis, for the 2-class classification problem. We use the axes (c) and (d) obtained in the unbiased case.

Similarly, Fig. 6 shows the phase diagrams predicted by the trained QCNN with the projection measurement onto the (a) XX-axis, (b) ZZ-axis, (c) high-accuracy axis and (d) optimized axis, for the 3-class classification problem. The purple, blue, green, and yellow regions correspond to the phases of SPT, Nothing, Paramagnetic, Antiferromagnetic, with the labels "0", "1", "2", and "3", respectively. The value of classification accuracy in each measurement methods are (a) 0.70, (b) 0.05, (c) 0.87, and (d) 0.68. As in the 2-class case, the optimal measurement (d) achieves less accurate detection of the phase, compared to (c) and even (a).

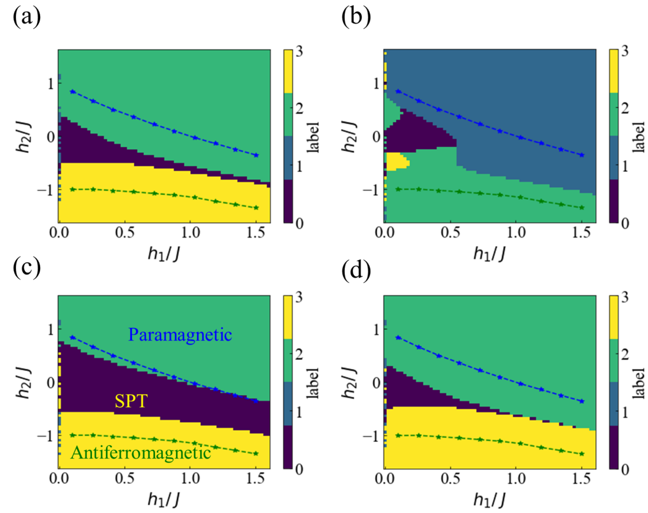

FIG. 6. Phase diagram predicted by the QCNN with the projection measurement onto the (a) XX-axis, (b) ZZ-axis, (c) high-accuracy axis, and (d) optimized axis, for the 3-class classification problem. We use the axes (c) and (d) obtained in the unbiased case.

VIII. Conclusion

We have proposed the quantum inception score as a quality measure of quantum generative models, and obtained the following three main claims by connecting to the Holevo information. First, the quantum coherence preserved in the classifier plays a central role in enhancing the quality of quantum generative models. Second, the best quality can be further achieved with the entanglement of the generator's output and joint measurement on the classifier. Third, the quality degradation of quantum generative models is due to the decoherence in the classifier, which can be quantified by the quantum efficacy emerging from the quantum fluctuation theorem. We also show examples of utilizing the quantum inception score to evaluate the quality of the 1D spin-1/2 chain as a generator, for the 2-class and 3-class classification of the quantum phase in the quantum many-body physics.

Finally we remark that, in the classical regime, IS is not currently a widely used measure for assessing generative models because of its potential constraints in facilitating useful model comparison as pointed out in Ref. [19]. These constraints could extend to the qIS in the similar manner. Nonetheless, the results obtained in this paper based on qIS enable us to emphasize the significance of further investigation of characterizing the quantum machine learning protocols from the fundamental perspectives, such as quantum information transmission and information thermodynamics.

Acknowledgement

We are grateful to Ryuji Takagi, Haidong Yuan, Paola Cappellaro, Mingda Li, Sebastian Deffner, Marco Cerezo, Quntao Zhuang and Tharon Holdsworth for insightful and helpful discussions. A.S. is supported by the NSF under Grant No. MPS-2328774. N.Y. is supported by MEXT Quantum Leap Flagship Program Grants No. JPMXS0118067285 and No. JPMXS0120319794 and JST Grant No. JPMJPF2221.

---

[1] I. Goodfellow, Y. Bengio, and A. Courville, *Deep learning* (MIT press, 2016).

[2] C. C. Aggarwal, Neural networks and deep learning, Springer **10**, 3 (2018).

[3] S. G. Finlayson, J. D. Bowers, J. Ito, J. L. Zittrain, A. L. Beam, and I. S. Kohane, Adversarial attacks on medical machine learning, Science **363**, 1287 (2019).

[4] B. Biggio and F. Roli, Wild patterns: Ten years after the rise of adversarial machine learning, in *Proc. ACM Conf. Comput. Commun. Secur.* (2018) pp. 2154–2156.

[5] A. Tanaka, A. Tomiya, and K. Hashimoto, *Deep Learning and Physics* (Springer, 2021).

[6] S. D. Sarma, D.-L. Deng, and L.-M. Duan, Machine learning meets quantum physics, Phys. Today **72**, 48 (2019).

[7] M. A. Nielsen and I. L. Chuang, *Quantum Computation and Quantum Information: 10th Anniversary Edition*, 10th ed. (Cambridge University Press, New York, NY, USA, 2010).

[8] K. T. Schütt, S. Chmiela, O. A. von Lilienfeld, A. Tkatchenko, K. Tsuda, and K.-R. Müller, Machine learning meets quantum physics, Lecture Notes in Physics (2020).

[9] J. Biamonte, P. Wittek, N. Pancotti, P. Rebentrost, N. Wiebe, and S. Lloyd, Quantum machine learning, Nature **549**, 195 (2017).

[10] S. Jerbi, L. J. Fiderer, H. Poulsen Nautrup, J. M. Kübler, H. J. Briegel, and V. Dunjko, Quantum machine learning beyond kernel methods, Nat. Commun. **14**, 517 (2023).

[11] G. Torlai and R. G. Melko, Machine-learning quantum states in the NISQ era, Annu. Rev. Condens. Matter Phys. **11**, 325 (2020).

[12] M. Schuld and F. Petruccione, *Machine learning with quantum computers* (Springer, 2021).

[13] H. B. Barlow, Unsupervised learning, Neural computation **1**, 295 (1989).

[14] H. U. Dike, Y. Zhou, K. K. Deveerasetty, and Q. Wu, Unsupervised learning based on artificial neural network: A review, in *2018 IEEE International Conference on Cyborg and Bionic Systems (CBS)* (IEEE, 2018) pp. 322–327.

[15] C. G. Turhan and H. S. Bilge, Recent trends in deep generative models: a review, in *2018 3rd International Conference on Computer Science and Engineering (UBMK)* (IEEE, 2018) pp. 574–579.

[16] J. Xu, H. Li, and S. Zhou, An overview of deep generative models, IETE Tech. Rev. **32**, 131 (2015).

[17] D. P. Kingma and M. Welling, An Introduction to Variational Autoencoders, Found. Trends Mach. Learn. **12**, 307 (2019).

[18] I. Goodfellow, J. Pouget-Abadie, M. Mirza, B. Xu, D. Warde-Farley, S. Ozair, A. Courville, and Y. Bengio, Generative adversarial networks, Commun. ACM. **63**, 139 (2020).

[19] S. Barratt and R. Sharma, A note on the inception score, arXiv preprint arXiv:1801.01973 (2018).

[20] T. Salimans, I. Goodfellow, W. Zaremba, V. Cheung, A. Radford, and X. Chen, Improved techniques for training gans, Adv. Neural. Inf. Process. Syst. **29** (2016).

[21] X. Gao, Z.-Y. Zhang, and L.-M. Duan, A quantum machine learning algorithm based on generative models, Sci. Adv. **4**, eaat9004 (2018).

[22] X. Gao, E. R. Anschuetz, S.-T. Wang, J. I. Cirac, and M. D. Lukin, Enhancing generative models via quantum correlations, Phys. Rev. X **12**, 021037 (2022).

[23] H. Tezuka, S. Uno, and N. Yamamoto, Generative model for learning quantum ensemble via optimal transport loss, arXiv preprint arXiv:2210.10743 (2022).

[24] J. Romero, J. P. Olson, and A. Aspuru-Guzik, Quantum autoencoders for efficient compression of quantum data, Quantum Sci. Technol. **2**, 045001 (2017).

[25] A. Khoshaman, W. Vinci, B. Denis, E. Andriyash, H. Sadeghi, and M. H. Amin, Quantum variational autoencoder, Quantum Sci. Technol. **4**, 014001 (2018).

[26] A. Pepper, N. Tischler, and G. J. Pryde, Experimental realization of a quantum autoencoder: The compression of qutrits via machine learning, Phys. Rev. Lett. **122**, 060501 (2019).

[27] H. Ma, C.-J. Huang, C. Chen, D. Dong, Y. Wang, R.-B. Wu, and G.-Y. Xiang, On compression rate of quantum autoencoders: Control design, numerical and experimental realization, arXiv:2005.11149 (2020).

[28] S. Lloyd and C. Weedbrook, Quantum generative adversarial learning, Phys. Rev. Lett. **121**, 040502 (2018).

[29] P.-L. Dallaire-Demers and N. Killoran, Quantum generative adversarial networks, Phys. Rev. A **98**, 012324 (2018).

[30] H.-L. Huang, Y. Du, M. Gong, Y. Zhao, Y. Wu, C. Wang, S. Li, F. Liang, J. Lin, Y. Xu, *et al.*, Experimental quantum generative adversarial networks for image generation, Phys. Rev. Appl. **16**, 024051 (2021).

[31] M. H. Amin, E. Andriyash, J. Rolfe, B. Kulchytskyy, and R. Melko, Quantum boltzmann machine, Phys. Rev. X **8**, 021050 (2018).

[32] C. Zoufal, A. Lucchi, and S. Woerner, Variational quantum boltzmann machines, Quantum Mach. Intell. **3**, 1 (2021).

[33] M. Kieferová and N. Wiebe, Tomography and generative training with quantum boltzmann machines, Phys. Rev. A **96**, 062327 (2017).

[34] W. Lian, S.-T. Wang, S. Lu, Y. Huang, F. Wang, X. Yuan, W. Zhang, X. Ouyang, X. Wang, X. Huang, *et al.*, Machine learning topological phases with a solid-state quantum simulator, Phys. Rev. Lett. **122**, 210503 (2019).

[35] H. Zhang, S. Jiang, X. Wang, W. Zhang, X. Huang, X. Ouyang, Y. Yu, Y. Liu, D.-L. Deng, and L.-M. Duan, Experimental demonstration of adversarial examples in

learning topological phases, Nat. Commun. **13**, 4993 (2022).
[36] D. Sels and E. Demler, Quantum generative model for sampling many-body spectral functions, Phys. Rev. B **103**, 014301 (2021).
[37] A. S. Holevo, Bounds for the quantity of information transmitted by a quantum communication channel, Probl. Pereda. Inf. **9**, 3 (1973).
[38] B. Schumacher and M. D. Westmoreland, Optimal signal ensembles, Phys. Rev. A **63**, 022308 (2001).
[39] H.-Y. Huang, M. Broughton, J. Cotler, S. Chen, J. Li, M. Mohseni, H. Neven, R. Babbush, R. Kueng, J. Preskill, and J. R. Macclean, Quantum advantage in learning from experiments, Science **376**, 1182 (2022).
[40] V. Vedral, An information–theoretic equality implying the Jarzynski relation, J. Phys. A: Math. Theor. **45**, 272001 (2012).
[41] A. Sone, N. Yamamoto, T. Holdsworth, and P. Narang, Jarzynski-like Equality of Nonequilibrium Information Production Based on Quantum Cross Entropy, Phys. Rev. Research **5**, 023039 (2023).
[42] D. Kafri and S. Deffner, Holevo's bound from a general quantum fluctuation theorem, Phys. Rev. A **86**, 044302 (2012).
[43] T. Sagawa and M. Ueda, Generalized Jarzynski equality under nonequilibrium feedback control, Phys. Rev. Lett. **104**, 090602 (2010).
[44] Y. Fujitani and H. Suzuki, Jarzynski equality modified in the linear feedback system, J. Phys. Soc. Jpn. **79**, 104003 (2010).
[45] I. Cong, S. Choi, and M. D. Lukin, Quantum convolutional neural networks, Nat. Phys **15**, 1273 (2019).
[46] E. Grant, M. Benedetti, S. Cao, A. Hallam, J. Lockhart, V. Stojevic, A. G. Green, and S. Severini, Hierarchical quantum classifiers, npj Quantum Inf. **4**, 65 (2018).
[47] P. Hausladen, R. Jozsa, B. Schumacher, M. Westmoreland, and W. K. Wootters, Classical information capacity of a quantum channel, Phys. Rev. A **54**, 1869 (1996).
[48] B. Schumacher and M. D. Westmoreland, Sending classical information via noisy quantum channels, Phys. Rev. A **56**, 131 (1997).
[49] A. S. Holevo, The capacity of the quantum channel with general signal states, IEEE Trans. Info. Theo. **44**, 269 (1998).
[50] C. King and M. B. Ruskai, Capacity of quantum channels using product measurements, J. Math. Phys. **42**, 87 (2001).
[51] A. S. Holevo, M. Sohma, and O. Hirota, Capacity of quantum Gaussian channels, Phys. Rev. A **59**, 1820 (1999).
[52] K. Siudzińska, Classical capacity of generalized pauli channels, J. Phys. A: Math. Theor. **53**, 445301 (2020).
[53] J. Lee, S.-W. Ji, J. Park, and H. Nha, Classical capacity of Gaussian communication under a single noisy channel, Phys. Rev. A **91**, 042336 (2015).
[54] L. Gyongyosi, S. Imre, and H. V. Nguyen, A survey on quantum channel capacities, IEEE Commun. Surv. Tutor. **20**, 1149 (2018).
[55] M. B. Hastings, Superadditivity of communication capacity using entangled inputs, Nat. Phys. **5**, 255 (2009).
[56] W. Li and D.-L. Deng, Recent advances for quantum classifiers, Sci. China: Phys. Mech. Astron. **65**, 220301 (2022).
[57] T. Hur, L. Kim, and D. K. Park, Quantum convolutional neural network for classical data classification, Quantum Mach. Intell. **4**, 3 (2022).
[58] N. Wrobel, A. Baul, J. Moreno, and K.-M. Tam, An application of quantum machine learning on quantum correlated systems: Quantum convolutional neural network as a classifier for many-body wavefunctions from the quantum variational eigensolver, arXiv preprint arXiv:2111.05076 (2021).
[59] G. Chen, Q. Chen, S. Long, W. Zhu, Z. Yuan, and Y. Wu, Quantum convolutional neural network for image classification, Pattern Anal. Appl. **26**, 655 (2023).
[60] R. Jozsa, D. Robb, and W. K. Wootters, Lower bound for accessible information in quantum mechanics, Phys. Rev. A **49**, 668 (1994).
[61] E. Davies, Information and quantum measurement, IEEE Trans. Inf. Theory **24**, 596 (1978).
[62] J. Watrous, *The Theory of Quantum Information* (Cambridge University Press, 2018).
[63] V. Vedral, The role of relative entropy in quantum information theory, Rev. Mod. Phys. **74**, 197 (2002).
[64] M. Lostaglio, K. Korzekwa, D. Jennings, and T. Rudolph, Quantum coherence, time-translation symmetry, and thermodynamics, Phys. Rev. X **5**, 021001 (2015).
[65] M. Lostaglio, D. Jennings, and T. Rudolph, Description of quantum coherence in thermodynamic processes requires constraints beyond free energy, Nat. Commun. **6**, 6383 (2015).
[66] I. Marvian and R. W. Spekkens, Asymmetry properties of pure quantum states, Phys. Rev. A **90**, 014102 (2014).
[67] I. Marvian, Coherence distillation machines are impossible in quantum thermodynamics, Nat. Commun. **11**, 25 (2020).
[68] I. Marvian, R. W. Spekkens, and P. Zanardi, Quantum speed limits, coherence, and asymmetry, Phys. Rev. A **93**, 052331 (2016).
[69] R. Takagi, Skew informations from an operational view via resource theory of asymmetry, Sci. Rep. **9**, 14562 (2019).
[70] K. Yamaguchi and H. Tajima, Smooth metric adjusted skew information rates, Quantum **7**, 1012 (2023).
[71] M. Ahmadi, D. Jennings, and T. Rudolph, The Wigner-Araki-Yanase theorem and the quantum resource theory of asymmetry, New J. Phys. **15**, 013057 (2013).
[72] G. Gour and R. W. Spekkens, The resource theory of quantum reference frames: manipulations and monotones, New J. Phys. **10**, 033023 (2008).
[73] I. Marvian and R. W. Spekkens, The theory of manipulations of pure state asymmetry: I. basic tools, equivalence classes and single copy transformations, New J. Phys. **15**, 033001 (2013).
[74] I. Marvian and R. W. Spekkens, Extending noether's theorem by quantifying the asymmetry of quantum states, Nat. Commun. **5**, 3821 (2014).
[75] G. Gour, I. Marvian, and R. W. Spekkens, Measuring the quality of a quantum reference frame: The relative entropy of frameness, Phys. Rev. A **80**, 012307 (2009).
[76] I. Marvian and S. Lloyd, From clocks to cloners: Catalytic transformations under covariant operations and recoverability, arXiv preprint arXiv:1608.07325 (2016).
[77] J. A. Vaccaro, F. Anselmi, H. M. Wiseman, and K. Jacobs, Tradeoff between extractable mechanical work, accessible entanglement, and ability to act as a reference system, under arbitrary superselection rules, Phys. Rev.

A **77**, 032114 (2008).
[78] S. D. Bartlett and H. M. Wiseman, Entanglement constrained by superselection rules, Phys. Rev. Lett. **91**, 097903 (2003).
[79] For a finite group, we have $\mathcal{G}(\rho) \equiv \frac{1}{|G|}\sum_{g\in G} U_g \rho U_g^\dagger$, where $|G|$ denotes the order of the group.
[80] J. Åberg, Quantifying superposition, arXiv preprint quant-ph/0612146 (2006).
[81] T. Baumgratz, M. Cramer, and M. B. Plenio, Quantifying coherence, Phys. Rev. Lett. **113**, 140401 (2014).
[82] For the origin of γ regarding the Holevo information, refer to Eqs. (11) – (14) in Ref. [42].
[83] M. B. Ruskai, Inequalities for quantum entropy: A review with conditions for equality, J. Math. Phys. **43**, 4358 (2002).
[84] A. Pesah, M. Cerezo, S. Wang, T. Volkoff, A. T. Sornborger, and P. J. Coles, Absence of barren plateaus in quantum convolutional neural networks, Phys. Rev. X **11**, 041011 (2021).
[85] A. Uvarov and J. D. Biamonte, On barren plateaus and cost function locality in variational quantum algorithms, J. Phys. A Math. Theor. **54**, 245301 (2021).
[86] J. R. McClean, S. Boixo, V. N. Smelyanskiy, R. Babbush, and H. Neven, Barren plateaus in quantum neural network training landscapes, Nat. Commun. **9**, 1 (2018).
[87] M. Cerezo, A. Sone, T. Volkoff, L. Cincio, and P. J. Coles, Cost-function-dependent barren plateaus in shallow quantum neural networks, Nat. Commun. **12**, 1791 (2021).
[88] S. Wang, E. Fontana, M. Cerezo, K. Sharma, A. Sone, L. Cincio, and P. J. Coles, Noise-induced barren plateaus in variational quantum algorithms, Nat. Commun. **12**, 1 (2021).
[89] B. Zhang, A. Sone, and Q. Zhuang, Quantum computational phase transition in combinatorial problems, npj Quantum Inf. **8**, 87 (2022).
[90] J. Jeyaretnam, J. Richter, and A. Pal, Quantum scars and bulk coherence in a symmetry-protected topological phase, Phys. Rev. B **104**, 014424 (2021).
[91] X. Chen, Y.-M. Lu, and A. Vishwanath, Symmetry-protected topological phases from decorated domain walls, Nat. Commun. **5**, 3507 (2014).
[92] F. D. M. Haldane, Nonlinear Field Theory of Large-Spin Heisenberg Antiferromagnets: Semiclassically Quantized Solitons of the One-Dimensional Easy-Axis Néel State, Phys. Rev. Lett. **50**, 1153 (1983).
[93] Z.-C. Gu and X.-G. Wen, Tensor-entanglement-filtering renormalization approach and symmetry-protected topological order, Phys. Rev. B **80**, 155131 (2009).
[94] F. Pollmann, E. Berg, A. M. Turner, and M. Oshikawa, Symmetry protection of topological phases in one-dimensional quantum spin systems, Phys. Rev. B **85**, 075125 (2012).
[95] J. C. Spall, An overview of the simultaneous perturbation method for efficient optimization, Johns Hopkins APL Tech. Dig. **19**, 482 (1998).
[96] J. C. Spall, Stochastic optimization: stochastic approximation and simulated annealing, Wiley Encyclopedia of electrical and electronics engineering **20**, 529 (1999).
[97] Specifically, we measure the output of the trained QCNN with some projectors and assign the label that corresponds to the highest probability of the measurement results.

A. Derivation of Eq. (25)

In this section, we provide the proof details of Eq. (25). We discuss two cases: nondegenerate and degenerate H.

1. Nondegenerate H

First, let us focus on the case that H is nondegenerate. H can be diagonalized as

$$H = \sum_{n=1}^{D} \omega_n |\omega_n\rangle\langle\omega_n| \,, \tag{A1}$$

where D denotes the dimension of the Hilbert space and $\{\omega_n\}_{n=1}^D$ are all different from each other. Here, $\{|\omega_n\rangle\}_{n=1}^D$ is an orthonormal basis of H. Defining,

$$\Delta\omega_{nm} \equiv \omega_n - \omega_m, \tag{A2}$$

we have

$$\begin{aligned}
\frac{1}{2T}\int_{-T}^{T} dt e^{-iHt}\rho e^{iHt} =& \frac{1}{2T}\sum_{n,m}\int_{-T}^{T} dt e^{-i\Delta\omega_{nm}t}\langle\omega_n|\rho|\omega_m\rangle|\omega_n\rangle\langle\omega_m| \\
=& \sum_{n,m} \mathrm{sinc}(\Delta\omega_{nm}T)\langle\omega_n|\rho|\omega_m\rangle|\omega_n\rangle\langle\omega_m| \\
=& \sum_{n=1}^{D}\langle\omega_n|\rho|\omega_n\rangle|\omega_n\rangle\langle\omega_n| + \sum_{n\neq m}\mathrm{sinc}(\Delta\omega_{nm}T)\langle\omega_n|\rho|\omega_m\rangle|\omega_n\rangle\langle\omega_m| \,,
\end{aligned} \tag{A3}$$

where we used $\mathrm{sinc}(0) = 1$. Then, by utilizing $\lim_{T\to\infty} \mathrm{sinc}(T\Delta\omega_{nm}) = 0$ ($\Delta\omega_{nm} \neq 0$), the second term vanishes when $T \to \infty$; therefore, we obtain

$$\mathcal{G}_H(\rho) = \lim_{T\to\infty}\left[\frac{1}{2T}\int_{-T}^{T} dt e^{-itH}\rho e^{itH}\right] = \sum_{n=1}^{D}\langle\omega_n|\rho|\omega_n\rangle|\omega_n\rangle\langle\omega_n| = \sum_{n=1}^{D}\Pi_n\rho\Pi_n\,, \tag{A4}$$

where $\Pi_n \equiv |\omega_n\rangle\langle\omega_n|$ is a rank-1 projector onto the eigenstate $|\omega_n\rangle$ of H. This implies that $\mathcal{G}_H$ corresponds to the dephasing map transferring ρ into a fully incoherent state [81] diagonal in the eigenbasis $\{|\omega_n\rangle\}_{n=1}^{D}$ of H. Then, the relative entropy of asymmetry $A(\rho; H) \equiv S(\rho\,\|\,\mathcal{G}_H(\rho))$ coincides with the relative entropy of coherence [81].

2. Degenerate H

Next, let us discuss the case that H is degenerate. Again, H can be diagonalized as Eq. (A1). Suppose that H has λ degenerate eigenvalues

$$\omega_{\alpha_1}, \omega_{\alpha_2}, \cdots, \omega_{\alpha_\lambda}\,. \tag{A5}$$

For each degenerate eigenvalue ω_{α_μ}, suppose that we have k_μ orthonormal eigenbasis

$$\{|\omega_{\alpha_\mu}^{(1)}\rangle, |\omega_{\alpha_\mu}^{(2)}\rangle, \cdots, |\omega_{\alpha_\mu}^{(k_\mu)}\rangle\}\,. \tag{A6}$$

Defining

$$\overline{K} \equiv \sum_{\mu=1}^{\lambda} k_\mu\,, \tag{A7}$$

the number of distinct nondegenerate eigenvalues is given by

$$K = D - \overline{K}\,. \tag{A8}$$

Then, $L = K + \lambda < D$ is the total number of distinct eigenvalues of H, and the Hilbert space can be written as

$$\mathcal{H} = \bigoplus_{\alpha=1}^{L}\mathcal{H}_\alpha\,, \tag{A9}$$

where $\mathcal{H}_\alpha$ denotes the subspace spanned by the eigenstates of H corresponding to the eigenvalue ω_α. Here, for the nondegenerate eigenvalue ω_α, the corresponding projector is the rank-1 projector

$$\Pi_{\omega_\alpha} \equiv |\omega_\alpha\rangle\langle\omega_\alpha|\,. \tag{A10}$$

For the degenerate eigenvalue ω_{α_μ}, the projector onto the corresponding subspace of the eigenbasis is

$$\Pi_{\alpha_\mu} = \sum_{\nu=1}^{k_\mu}|\omega_{\alpha_\mu}^{(\nu)}\rangle\langle\omega_{\alpha_\mu}^{(\nu)}|\,, \tag{A11}$$

so that the rank of the projector is $\mathrm{rank}(\Pi_{\alpha_\mu}) = k_\mu > 1$. Now, let us define the set of the nondegenerate eigenvalues as

$$\Omega \equiv \{\omega_\alpha\,|\,\omega_\alpha \neq \omega_\beta,\ \alpha \neq \beta\} \tag{A12}$$

and the set of degenerate eigenvalues as

$$\Gamma \equiv \{\omega_\alpha\,|\,\omega_\alpha = \omega_\beta, \alpha \neq \beta\}\,. \tag{A13}$$

Then, we have

$$
\begin{aligned}
\frac{1}{2T}\int_{-T}^{T} dt e^{-iHt}\rho e^{iHt} &= \sum_{n,m} \mathrm{sinc}(\Delta\omega_{nm}T)\langle\omega_n|\rho|\omega_m\rangle|\omega_n\rangle\langle\omega_m| \\
&= \sum_{\omega_\alpha\in\Omega}\langle\omega_\alpha|\rho|\omega_\alpha\rangle|\omega_\alpha\rangle\langle\omega_\alpha| + \sum_{\omega_\alpha,\omega_\beta\in\Gamma}\langle\omega_\alpha|\rho|\omega_\beta\rangle|\omega_\alpha\rangle\langle\omega_\beta| \\
&\quad + \sum_{\omega_\alpha,\omega_\beta\in\Omega}\mathrm{sinc}(\Delta\omega_{\alpha\beta}T)\langle\omega_\alpha|\rho|\omega_\beta\rangle|\omega_\alpha\rangle\langle\omega_\beta| \\
&= \sum_{\omega_\alpha\in\Omega}\langle\omega_\alpha|\rho|\omega_\alpha\rangle|\omega_\alpha\rangle\langle\omega_\alpha| + \sum_{\mu=1}^{\lambda}\sum_{\nu=1}^{k_\mu}\sum_{\nu'=1}^{k_\mu}\langle\omega_{\alpha_\mu}^{(\nu)}|\rho|\omega_{\alpha_\mu}^{(\nu')}\rangle|\omega_{\alpha_\mu}^{(\nu)}\rangle\langle\omega_{\alpha_\mu}^{(\nu')}| \\
&\quad + \sum_{\omega_\alpha,\omega_\beta\in\Omega}\mathrm{sinc}(\Delta\omega_{\alpha\beta}T)\langle\omega_\alpha|\rho|\omega_\beta\rangle|\omega_\alpha\rangle\langle\omega_\beta| \\
&= \sum_{\omega_\alpha\in\Omega}\Pi_{\omega_\alpha}\rho\Pi_{\omega_\alpha} + \sum_{\mu=1}^{\lambda}\Pi_{\alpha_\mu}\rho\Pi_{\alpha_\mu} + \sum_{\omega_\alpha,\omega_\beta\in\Omega}\mathrm{sinc}(\Delta\omega_{\alpha\beta}T)\langle\omega_\alpha|\rho|\omega_\beta\rangle|\omega_\alpha\rangle\langle\omega_\beta|,
\end{aligned}
\tag{A14}
$$

where the third term vanishes as $T\to\infty$. Therefore, defining the set of projectors

$$
\{\Pi_n\}_{n=1}^{L} \in \{\Pi_{\omega_\alpha}\}_{\omega_\alpha\in\Omega} \cup \{\Pi_{\alpha_\mu}\}_{\mu=1}^{\lambda} \tag{A15}
$$

onto the subspace of the eigenbasis of H,we obtain Therefore, we have

$$
\mathcal{G}_H(\rho) = \lim_{T\to\infty}\left[\frac{1}{2T}\int_{-T}^{T} dt e^{-itH}\rho e^{itH}\right] = \sum_{n=1}^{L}\Pi_n\rho\Pi_n\,, \tag{A16}
$$

which is a block diagonal state. In this case, the relative entropy of asymmetry $A(\rho;H)\equiv S\left(\rho\,\|\,\mathcal{G}_H(\rho)\right)$ coincides with the relative entropy of superposition [80]. Obviously, Eq. (A16) is reduced to Eq. (A4) when we have $\mathrm{rank}(\Pi_{\alpha_\mu}) = 1$ $(\forall\mu)$, which corresponds to the case that H is nondegenerate.